

Energy & Environmental Science

Accepted Manuscript



This is an *Accepted Manuscript*, which has been through the Royal Society of Chemistry peer review process and has been accepted for publication.

Accepted Manuscripts are published online shortly after acceptance, before technical editing, formatting and proof reading. Using this free service, authors can make their results available to the community, in citable form, before we publish the edited article. We will replace this *Accepted Manuscript* with the edited and formatted *Advance Article* as soon as it is available.

You can find more information about *Accepted Manuscripts* in the [Information for Authors](#).

Please note that technical editing may introduce minor changes to the text and/or graphics, which may alter content. The journal's standard [Terms & Conditions](#) and the [Ethical guidelines](#) still apply. In no event shall the Royal Society of Chemistry be held responsible for any errors or omissions in this *Accepted Manuscript* or any consequences arising from the use of any information it contains.

Cite this: DOI: 10.1039/c0xx00000x

www.rsc.org/xxxxxx

ARTICLE TYPE

Small-sized and high-dispersed WN from $[\text{SiO}_4(\text{W}_3\text{O}_9)_4]^{4-}$ clusters loading on GO-derived graphene as promising carriers for methanol electro-oxidation

Haijing Yan, Chungui Tian*, Li Sun, Bo Wang, Lei Wang, Jie Yin, Aiping Wu and Honggang Fu*

5 Received (in XXX, XXX) Xth XXXXXXXXXX 20XX, Accepted Xth XXXXXXXXXX 20XX
DOI: 10.1039/b000000x

The small size and high dispersion of cocatalysts on supports are essential to increase the chance to contact with Pt catalyst for promoting the synergistic effect. In this paper, we report the synthesis of the small-sized WN nanoparticles (NPs) loading on the GO-derived graphene (denoted as graphene for simplicity) by using heteropoly acid $\text{H}_4[\text{SiO}_4(\text{W}_3\text{O}_9)_4]$ (SiW_{12}) clusters as W source. The SiW_{12} clusters are anchored on the polyethyleneimine (PEI)-modified GO through a hydrothermal process. After the nitridation with NH_3 , the small-sized and well dispersed WN NPs of 2-3 nm are obtained. The ternary Pt-WN/graphene catalyst are fabricated by an EG reduction method. The intimate contact and intensive interaction between Pt and WN are verified by TEM, XRD, XPS and XAFS tests. Due to the characteristics above, the Pt-WN/graphene catalyst exhibits a remarkably enhanced activity and durability toward methanol electrocatalytic oxidation. The mass activity of Pt-WN/graphene ($531.5 \text{ mA mg}^{-1}_{\text{Pt}}$) is 2.45, 2.88 and 3.70 times of Pt/graphene, Pt/C(JM) and Pt/Vulcan catalysts. Furthermore, the ternary Pt-WN/graphene catalyst shows excellent resistance to CO poisoning and good stability. The high activity of Pt-WN/graphene is mainly attributed to the enhanced synergistic effect benefited from the intimate contact and intensive interaction of Pt with WN NPs.

Introduction

20 Direct methanol fuel cells (DMFC), a kind of polymer electrolyte fuel cells, are attracting much more attention in clean energy technology due to its high energy density, high efficiency and cleanliness, easy storage and transportation of liquid methanol at ambient conditions.^[1] The Pt metal is current state-of-the-art catalytic materials, but suffers from the prohibitive high cost of Pt and the decrease of catalytic activity over time.^[2] The development of inexpensive catalysts (decrease of usage or replacement of Pt with other metal) is thus of great importance for the commercialization of DMFC. For the cathodic oxygen reduction reaction (ORR), the replacement of Pt metal with non-noble metal catalysts, such as (doped) carbon nanotube^[3a,3b], graphene^[3c,3d] and cobalt porphyrin,^[4] is potential solution to the problems. While for the anode oxidation reaction, it is difficult to completely replace Pt with non-metal catalysts. The alloying with other metals, such as Ru, Ni, Cu, is popular way to decrease the usage of Pt metal and improve the ability to CO poisoning via the bifunctional mechanism.^[5] Unfortunately, the alloying metal in catalyst is easy to dissolve out during the methanol electro-oxidation process, resulting the low stability and decrease of the catalytic activity of the catalysts.^[5b] It will be desirable to design the low-Pt catalyst with the high activity and good stability.

Transition metal nitrides (carbides) have attracted considerable interest in material science because of their unique properties for technological applications.^[6,7] In the field of DMFC, the carbides (nitrides) are considered to be promising co-catalyst of Pt metal due to the unique electric properties and high stability.^[8] The experimental and theoretical studies have indicated that the carbides (WC) can be used as effective and stable co-catalysts of

Pt metal to facilitate the methanol oxidation, and thus to improve the utilization and increasing the tolerance of Pt to CO poisoning via a "synergistic action" mechanism^[9, 10] In view of the similar structure of traditional metal nitrides and carbides,^[11] the nitrides (for example, WN) should be a good co-catalyst in electrochemical reaction for DMFC. The studies have indicated that the VN and Fe_2N can be used as catalyst or co-catalyst of Pt for catalyzing ORR reaction.^[12a,b] Li and co-workers have also found the potential application of TiN for catalyzing ORR reaction.^[12c] Besides, in some reactions, the nitrides (Mo_2N) are more active than carbide (Mo_2C).^[13] Although relative less studies than the carbide counterparts, the works imply already the large potential of nitrides in electrocatalytic fields. In this case, the good co-catalytic efficiency can be contributed the unique properties of nitrides, but severely effected by the size and dispersion of the particles on supports. The small size and uniform distribution can increase largely the chance of nitrides to contact with Pt, which would be important for the development of the synergistic catalytic action. However, the practical preparation of the nitrides with these characteristics remains a large challenge to data. The traditional syntheses for the nitrides, including temperature-programmed reaction route and direct impregnation method,^[14-18] either suffer incomplete ammonification (leaving behind un-reacted metals) or crystal growth (large size of the particles), which are not favorable for developing the co-catalytic action of nitrides. To decrease the size of nitrides and stabilize the particles from aggregation in reaction and application, it is necessary to load the nitrides (carbide) on certain supports, such as silica and carbon. The process includes usually loading a precursor on supports, followed by nitridation in NH_3 atmosphere. Obviously, the size and dispersion of

precursor on carriers will play predominant role on the characteristics of resulted nitrides. Unfortunately, the traditional direct impregnation route can result the relatively large size and uneven distribution of WN NPs on supports, mainly due to the difficulty in controlling the size and dispersion of W precursor. If the W source can be distributed on the support with small size and good uniformity, it is quite possible to achieve small-sized and evenly dispersed nitrides NPs. However, it remains still a big challenge to date.

Polyoxometalates (POMs) are known as a famous class of molecular clusters with much diversity in size, composition and function. The most attractive features of POMs are small size close to the nanometer level and stable structure.^[19] The high electric charge and good solubility of POMs clusters make them easy coordination with other substrates to form small-sized and uniform clusters.^[20] The characteristics of POMs imply their potential to act suitable precursor for small-size nitrides. In this paper, we reported a versatile assembly method for the synthesis of small-sized nitrides NPs about 2-3 nm loaded on GO-derived graphene. The WN from $H_4[SiO_4(W_3O_9)_4]$ (SiW_{12}) clusters was selected as a representative. The graphene, a two-dimensional carbon material, has been demonstrated as a good support for loading functional particles for electrochemical application.^[21] The previous works have indicated that the metal NPs loaded on the graphene can show the good performance for the electro-oxidation of fuel molecules^[22a-c] and ORR.^[22d] Thus, the growth of the small-sized and high-dispersed POMs clusters, and final transformation of them into small-sized nitrides with good dispersion on graphene will give a high effective co-catalyst of Pt in electrocatalytic reaction. In our synthesis, the graphite oxides (GO) were selected as the precursor of graphene based on their virtue of easily preparation in large quality and plentiful groups. The direct growth of POMs on graphene will result in the formation of uneven particles because the negative charges of both POMs anions and the GO are not favorable for the assembly of them. To overcome this problem, the GO was first modified with positive charged polyethyleneimine (PEI). Then, SiW_{12} clusters were anchored on PEI-modified GO through a hydrothermal assembling process. Due to the intensive interaction of negative charged SiW_{12} anions and positive charged PEI-modified GO, the SiW_{12} clusters can be anchored on the GO with small size and well dispersion. After nitriding, the WN NPs with small size of 2-3 nm and good dispersion can be formed on GO-derived graphene. Our results indicated that WN/graphene can act a promising support of Pt NPs for electrooxidation reaction of methanol. It is found that the existence of the intimate contact and intensive interaction between Pt and WN in the ternary catalyst as shown by XPS, XRD, TEM and XAFS tests. The ternary catalyst is characterized by its high activity (the mass activity is 2.45, 2.88 and 3.70 times of Pt/graphene, commercial Pt/C(JM) and home-made Pt/Vulcan catalysts), excellent resistance to CO poisoning and good stability. The excellent performance of Pt-WN/graphene is relative with the small size and high dispersion of WN on graphene, which increase largely the chance of WN to contact with Pt catalyst for promoting the synergistic effect.

Experimental Section

Chemicals. The $H_4[SiO_4(W_3O_9)_4]$ (SiW_{12}), H_2PtCl_6 , ethanol (C_2H_5OH) was purchased from Tianjin Kermel Chemical

Reagent Co., Ltd. The polyethyleneimine (PEI, MW: 600000-1000000) was purchased from Fluka. All reagents were used as received without further purification.

Preparation of PEI modified GO (PEI-GO)

Graphite oxide (GO) was synthesized from graphite by a modified Hummer's method.^[23] To make the effective assembly of SiW_{12} with GO support, the GO was firstly modified with positive charge PEI. The GO sheets (80 mg) were dispersed in water of 20 mL to form a stable dispersion (4 mg mL^{-1}) in an ultrasonic bath for 10 min. The GO dispersion was mixed with 20 mL of 4 mg mL^{-1} poly(ethyleneimine) (PEI) aqueous solution under stirring. After the mixed solution was stirred 24 h, the excess polymer was removed by repeated centrifugation (4500 rpm, 5 min) and washing cycles. The PEI-GO was dispersed in deionized (DI) water for compounding with SiW_{12} .

Preparation of SiW_{12} /PEI-graphene and WN/graphene

To anchor the SiW_{12} on PEI-GO, SiW_{12} (0.08 g) in deionized water (40 mL) was added dropwise into the PEI-GO solution of 40 mL (2 mg/mL) under vigorously stirring. After stirring for 24h, the mixture was transferred into a 100 mL Teflon-lined autoclave and hydrothermally treated at $180 \text{ }^\circ\text{C}$ for 10 h. The resulting solid (black) was collected by centrifugation, and washed repeatedly with deionized water and alcohol. The hydrothermal treatment can result in the partial reduction of GO to GO-derived graphene (denoted as graphene for simplicity). So, the resulted product was denoted as SiW_{12} /PEI-graphene that was dried at $60 \text{ }^\circ\text{C}$ in a vacuum oven for 6 h. The black color indicates also the transformation of GO to GO-derived graphene under hydrothermal reaction. Before nitridation, the SiW_{12} /PEI-graphene was calcined at $300 \text{ }^\circ\text{C}$ for 5 h to obtain WO_3 /graphene (PEI were omitted for clarification). The WO_3 /graphene was then heated at 800°C with a heating rate of $5 \text{ }^\circ\text{C}\cdot\text{min}^{-1}$ under NH_3 atmospheres and maintained at $800 \text{ }^\circ\text{C}$ for 3 h. After slow cooling to room temperature under an N_2 atmosphere, the WN/graphene was obtained.

Loading Pt on WN/graphene to form Pt-WN/graphene

Pt-WN/graphene was formed by loading Pt on WN/graphene by a ethylene glycol (EG) method.^[24] Typically, 50 mg of WN/graphene support was dispersed in 50 mL EG by ultrasonication. Then, an appropriate amount EG solution of H_2PtCl_6 was add to the suspension dropwise and magnetically stirred for 1 h, and 1.0 mol L^{-1} NaOH/EG solution was then added to adjust the pH of the suspension to 10. The slurry was heated at 250°C for 30 min. After placing at room temperature for 3 h, the product was filtrated, washed, and finally dried at 60°C for 24 h. The content of Pt in Pt-WN/graphene was about 7.5 wt%. As control, a graphene-supported Pt catalyst (Pt/graphene) was also prepared. The graphene support was prepared by hydrothermal treatment of GO under similar conditions with SiW_{12} /PEI-graphene composite. In addition, the Pt/Vulcan XC-72 (20 wt% Pt), commercial 20wt% Pt/carbon black (Johnson Matthey) and Pt black (Johnson Matthey), labeled Pt/Vulcan, Pt/C(JM) and Pt black (JM), respectively, are used as references.

Physical Characterizations

The morphology and structure of the samples were analyzed by scanning electron microscopy (SEM: Hitachi S-4800) with an acceleration voltage of 5 kV and transmission electron microscopy (TEM: JEM-2100) with an acceleration voltage of

200 kV. Carbon-coated copper grids were used as sample holders for TEM analysis. The electron energy loss spectroscopy (EELS) study was performed on FEI Tecnai F20 TEM with the acceleration voltage of 200 kV. Spectra were recorded with the Gatan GIF Quantum with an energy resolution of 0.9 eV. XPS (X-ray photoelectron spectroscopy) analysis was performed on a VG ESCALABMK II with a Mg K α achromatic X-ray source (1253.6 eV). The XAFS data at W L3-edge were measured at room temperature in transmission mode at beamline BL14W1 of Shanghai Synchrotron Radiation Facility (SSRF), China. X-ray diffraction (XRD) patterns were obtained on a Bruke D8 diffractometer using Cu K α ($\lambda=1.5406$ Å) radiation. The accelerating voltage and the applied current were 40 kV and 20 mA, respectively. Raman measurement was performed with a Jobin Yvon HR 800 micro-Raman spectrometer at 457.9 nm. Fourier transform infrared spectrum (FTIR) was collected in a NICOLETiS10 Spectrometer. The N₂ adsorption-desorption isotherms of as-made samples were conducted by using a Micromeritics Tristar II. The samples were outgassed for 10 h at 150 °C under vacuum before the measurements.

Electrochemical measurements

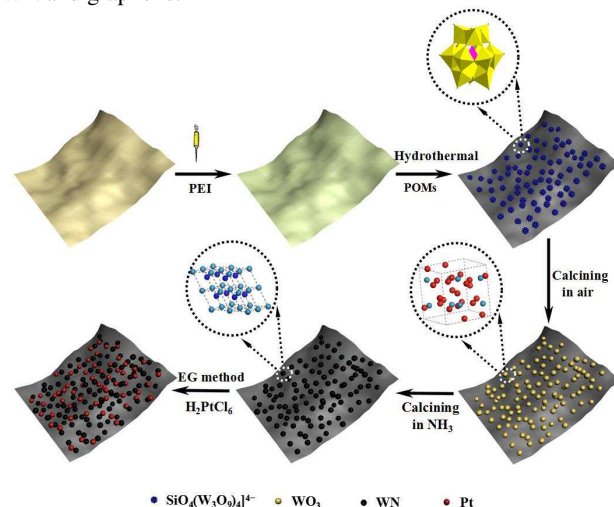
Electrochemical measurements were performed with a BAS100B electrochemical workstation. The conventional three-electrode cell was used for electrochemical test, in which the Pt plate acted as a counter electrode, saturated Hg/Hg₂Cl₂ electrode as a reference electrode and a glassy carbon (GC) electrode with 0.4 cm diameter as working electrode that was polished with 30 nm Al₂O₃ paste and washed with water and isopropanol. Five milligrams of catalyst was mixed with 50 μ L of 5 wt % Nafion ionomer and then was dispersed in 0.1 mL of isopropanol solution. After the catalyst ink was sonicated for 0.5 h, a volume of the ink was dropped on the GC electrode and left to dry. Nitrogen was bubbled through the solution for 30 min prior to the measurement with the purpose of deaeration. To evaluate the activity of the catalyst toward the methanol electrooxidation, an electrolyte of 1 M CH₃OH dissolved in 1 M H₂SO₄ solution was used. CO stripping measurement was performed as follows: after purging the solution with N₂ for 20 min, CO was bubbled for 15 min to form a CO adsorbed layer on the catalysts while maintaining the potential at -0.15V. Excess CO in solution was purged with N₂ for 20 min and CO stripping curve was recorded in H₂SO₄ solution at 20 mV s⁻¹. All electrochemical studies were carried out at 25 °C.

Results and Discussion

4.5 Characterization of WN/graphene and Pt-WN/graphene

The WN/graphene is prepared by firstly anchoring the SiW₁₂ on PEI-GO, followed by nitridation in NH₃ atmosphere. After the growth of Pt on the WN/graphene, the ternary Pt-WN/graphene catalyst is formed. The process is shown in Scheme 1. The PEI is a polymer with positive charge in which plentiful amine groups can bond with negatively charged colloids and ions.^[25] So, after mixing, the positively charged PEI can bond with GO through the coordination of amine with -OH (or COOH) bearing by GO, to form PEI-GO with positive surface charge (Step 1). In water, the H₄[SiO₄(W₃O₉)₄] can easily ionize to form a discrete, negatively charged heteropoly anion [SiO₄(W₃O₉)₄]⁴⁻. The anions can combine with amine in PEI-GO to obtain SiW₁₂/PEI-GO complex. A further hydrothermal treatment can promote the

assembly of SiW₁₂ with PEI-GO and reduce GO to graphene (SiW₁₂/PEI-graphene, Step 2). Subsequently, the SiW₁₂/PEI-graphene samples were calcined at 300 °C in air to generate dispersed WO₃ on graphene (Step 3). Due to intensive interaction of SiW₁₂ clusters with substrate, the small-sized WO₃ NPs can be generated. After calcining at 800 °C in NH₃, the small-sized WN NPs loading at graphene were obtained (Step 4). Loading Pt NPs on the WN/graphene support results in the final formation of the ternary Pt-WN/graphene composite (Step 5). The small size of WN should be relative with the small size and stable structure of POMs precursor, the anchoring function of amine groups on POMs clusters,^[26] as well as covalent interaction between final WN and graphene.^[27]



Scheme 1. The procedure for the synthesis of Pt-WN/graphene catalyst.

Raman spectra can provide useful information about the crystallinity of carbon and the formation of W compounds (Figure S1). Specifically, we can observe the large improvement of carbon crystallinity (high I_G/I_D) after the formation of WO₃/graphene sample. This is due to that the calcination can remove the oxygenous group of GO, and improve the crystallinity of GO, thus resulting in the formation of GO-derived graphene. However, the ratio of I_G/I_D decreases largely after the formation of WN/graphene, which can be ascribed to the disordered structure induced by intensive interaction of WN and graphene, and the doping of graphene by N heteroatoms under NH₃ atmosphere.^[28a] In addition, the 2D peaks can be observed at 2723 cm⁻¹, implying the formation of multilayer graphene as demonstrated by Ferrari et. al.^[28b] The peaks located at 813 cm⁻¹ for WO₃/graphene) and 820 cm⁻¹ for WN/graphene are ascribed to the stretching modes of the O-W-O^[29] and W-N bond,^[30] respectively. The infrared (IR) spectra of the samples from the different steps are displayed in Figure S2. For comparison, the IR spectrum of highly ordered pyrolytic graphite (HOPG) is also given. The peak located at about 3400cm⁻¹ is ascribed to the adsorption of H₂O. No intensive peaks can be observed in other region. However, we can see that the original GO shows many peaks corresponding to -OH, -COOH. After the modification with PEI, the peak ascribed to C=O-N emerge at 1500 cm⁻¹.^[31] For SiW₁₂/PEI-GO sample, the characteristic peaks located at 790 (W-O-W), 914 (W=O), 1144 cm⁻¹ (Si-O)^[32] for SiW₁₂ can be found, indicating the anchorage of SiW₁₂ on PEI-GO. The peaks

corresponding to the W-O bond can also be observed in $\text{WO}_3/\text{graphene}$ sample. However, after the nitridation reaction, the peaks belonging to W-O-W at 790 cm^{-1} disappear. A broad peak at 1141 cm^{-1} , ascribing to the vibration of W-N bond, can be observed. IR and Raman spectra imply the successful modification of different components on GO and graphene at different steps, the transformation of SiW_{12} to WO_3 and finally to WN through the POM-based route.

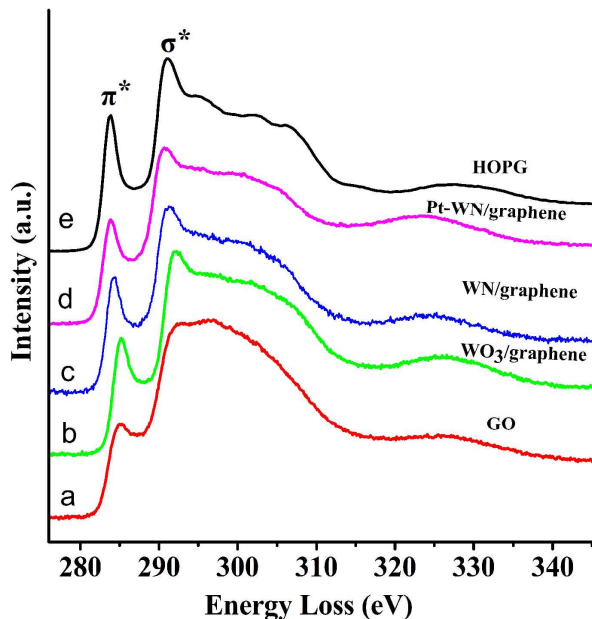


Figure 1. Carbon-K-ionization edges of (a) GO, (b) $\text{WO}_3/\text{graphene}$, (c) WN/graphene, (d) Pt-WN/graphene and (e) HOPG.

Table 1 sp^2/sp^3 quantification

	$\text{Nsp}^2(\%)$	$\text{Nsp}^3(\%)$
GO	61	39
$\text{WO}_3/\text{graphene}$	90	10
WN/graphene	86	14
Pt-WN/graphene	83	17
HOPG	100	0

The EELS is performed to identify the chemical state of carbon materials deeply. The highly ordered pyrolytic graphite (HOPG) is used as a standard for the sp^2 quantification. In the EELS spectra, the peak at 285 eV (labeled π^*) stems from transitions to the unoccupied antibonding π^* -states, while the intensive peaks at 292 eV is ascribed to the transitions to antibonding σ^* -states (σ^*). The $\text{sp}^2\%$ is calculated by formula S1.^[33] The EELS analysis indicates the existence of sp^2 carbon in the typical samples, including original GO, $\text{WO}_3/\text{graphene}$, WN/graphene and Pt-WN/graphene. The $\text{Nsp}^2\%$ is about 61%, 90%, 86% and 83% for GO, $\text{WO}_3/\text{graphene}$, WN/graphene and Pt-WN/graphene as shown in Figure 1 and Table 1. We can see the obvious increase of $\text{Nsp}^2\%$ in our samples. The results indicate that the crystallinity of carbon is increased in the order of $\text{WO}_3/\text{graphene} > \text{WN/graphene} > \text{Pt-WN/graphene} > \text{GO}$, being

inconsistent with the results of Raman analysis. The higher Nsp^2 in Pt-WN/graphene indicates the restoration of sp^2 carbon in GO in the synthesis, furtherly demonstrating the formation of the GO-derived graphene.

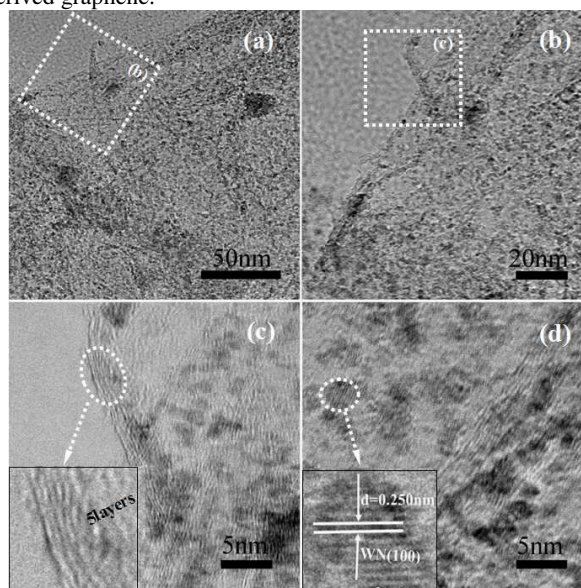


Figure 2. (a, b) low-magnified TEM images and (c, d) HRTEM of the WN/graphene.

The microstructure of WN/graphene is studied by SEM and TEM methods. From SEM image, we can observe the thin and separated graphene layer (Figure S3a). The formation of the discrete graphene sheets should be relative with the growth of WN on graphene, which can act a space for separating graphene from stack. However, we can not observe the WN NPs on graphene sheets. The results should be explained by the too small size of WN NPs to be observed by SEM test. From different low-magnification of TEM images in Figure 2a, b, we can see the small NPs with uniform size and good dispersion on graphene. The particles are 2-3 nm in size as shown by large-magnified TEM image in Figure 2c. It can also be clearly seen that the margin of carbon sheets is about 5 layers in thickness, indicating the formation of thin graphene sheets. The high-resolution TEM (HRTEM) image shows the distance of two adjacent planes of single particle is about 0.25 nm, corresponding to the (100) crystal facet of the hexagonal WN (Figure 2d). TEM and HRTEM images in Figure S4 indicate furtherly the formation of WN/graphene. Above tests demonstrate the formation of WN/graphene composites, in which the WN NPs have small size of 2-3 nm and good dispersion on graphene support. Previously, the nitrides can be obtained by solid-state ion exchange route, which can result in the formation of nitrides with large size above μm and poor dispersion.^[34] Yao and co-workers have loaded the MoN NPs on CNTs support through an impregnation technique by using $(\text{NH}_4)_6\text{Mo}_7\text{O}_{24}\cdot 4\text{H}_2\text{O}$ as Mo source.^[35] The nitrides as-prepared have a large size above 20 nm, and the distribution of them on CNTs is not uniform. Our group has also designed the VN/carbon composites with the size of VN about 20 nm through an ions-exchange method.^[12b] The nitrides with the small size of 2-3 nm have not been reported to data. The size of WN is also much smaller than that of corresponding carbides from either the impregnation route or ions-exchange method.^[36, 37] The formation

of the small-sized WN by our strategy should be contributed the followed factors: 1) the small size close to the nanometer, stable structure of POMs clusters make them suitable precursor of WN with small size; the W (Mo) sources used in many previous works are $(\text{NH}_4)_6\text{W}_7\text{O}_{24}$, $(\text{NH}_4)_6\text{Mo}_7\text{O}_{24}$ that has poor solubility in solvent, and NaWO_4 that is just a small molecular but not a cluster.^[37] Compared with those sources, the POMs have good solubility in many solvent, large size and stable structure, thus process many unique advantages for WN synthesis; 2) the anchoring function of PEI that are pre-modified on GO are also key for the formation of the small-sized WN. The direct mixing of SiW_{12} with GO can result the formation of the nitride with large size above 70 nm (Figure S5). These is due to the negative charge of both SiW_{12} clusters and GO, making them insufficient combination thus resulting in the formation of large and uneven particles. The PEI is a polymer with positive charge in which plentiful amine groups can bond with negatively charged colloids and ions. They can be used for construct the stable POM-based film by L-B-L techniques, based on the strong interaction of PEI with POMs ions.^[38] Thus, by PEI modification, the POMs ions can be anchored and stabilized on GO supports thus form the small-sized precursor. In XRD patterns of SiW_{12} /graphene and WO_3 /graphene samples, we can observe the several peaks corresponding to SiW_{12} and WO_3 (Figure S6). After nitridation, the precursor can be transformed into small-sized nitrides. X-ray diffraction (XRD) pattern of WN/graphene is shown in Figure S7 (curve a). The peak at 26.48° is characteristic of the parallel graphene sheets. The weak intensity implies less layers of graphene, being consistent with TEM and SEM observation. The thin graphene should be due to that WN embed in the graphene could prevent aggregation of graphene. The distinct diffraction peaks located at 37.64° , 43.76° , 63.67° and 76.48° are indexed to (100), (101), (210) and (102) reflections of hexagonal WN phase (Figure 2a). No other diffraction peaks are detected, indicating the high purity of WN phase. For the samples from the hydrothermal treatment of GO, the intensive peak at 26.48° can be observed (Figure S8a). In WN/graphene sample prepared by using GO without PEI modification as support, the metal W phase can be observed in addition to WN phase (Figure S8b). This result implies the important role of PEI on the formation of phase-pure WN.

The nitrides are good co-catalyst of Pt for electrocatalytic application. A traditional EG reduction method is use to load the Pt catalyst on WN/graphene support. From SEM image in Figure S3b, we can see discrete graphene thin sheets. However, being different with WN/graphene, we can see obviously the many small particles (white dots) on graphene sheets for this Pt-WN/graphene composite. The distinct white dots should be relative with the high conductivity of Pt NPs. Figure 3 shows the TEM images of Pt-WN/graphene composite. We can see many small particles below 5 nm in size on graphene sheets (Figure 3a, b). The HRTEM image of Pt-WN/graphene in Figure 3c shows small-sized particles close contact each other on graphene. The inset of Figure 3c displays the well-defined lattice fringes of the (100) crystal plane of WN in one area, and the (200) crystal plane of Pt NPs in adjacent areas surrounding WN. The Fast Fourier Transform (FFT) image (Figure 3d) shows two different distance of 0.0081 and 0.01001 nm corresponding to the (100) crystal

plane of WN and (200) crystal plane of Pt, being consistent with the HRTEM image. The images reveal the co-existence of Pt and WN in the composites. Importantly, it shows distinctly the intimate contact of Pt with WN, which should be largely favorable to promote the “synergistic effect” of them for high effective electrocatalysis. For Pt/graphene composite, the particle size of Pt NPs is above 10 nm (Figure S9), much larger than that of ternary composites (below 5 nm). The large size are not favorable for the full development of the catalytic activity of metal NPs.^[39] The results also reflect the intensive interaction of WN with Pt NPs. That is, the anchoring role of small-sized and well dispersed WN is favorable to form the small sized Pt NPs. Notably, by comparison of TEM image before (Figure 2) and after loading Pt (Figure 3), it can be found that the distribution of the WN NPs is changed before and after loading Pt. That is, the re-distribution of WN NPs occurs after loading Pt NPs. In previous work, we find that the presence of carbide can largely improved the crystallinity of Pt NPs because of the intensive interaction of WC with Pt NPs.^[27] Due to the similar structure of WC and WN, this interaction also exists between the WN and Pt NPs, thus resulting in a re-distribution of WN NPs after loading Pt NPs. The interaction of Pt with WN is also demonstrated by XRD analysis. As shown in Figure S7 (curve b), the peaks located at 39.7° , 46.2° and 67.5° can be identified as the (111), (200) and (220) reflections of a Face-centered cubic (fcc) structured Pt. However, the peaks belonging WN weakened for the ternary composites. The similar results are also observed for Pt-WC/carbon^[40] and Pt-Mo₂C/carbon.^[41] The filled states of the W d band are narrowed after nitride formation, resulting in similar electronic structures of nitrides with Pt metal up to the Fermi level. So, the observation can be explained by intensive interaction of Pt with WN NPs and epitaxial grown of Pt on WN due to the similar electronic structures. Also, the Pt (111)/(200) and WN(100)/(101) overlap in XRD pattern, and thus we can not observed single peaks of WN. The interaction between Pt and WN is more advantageous for the application in advanced areas.

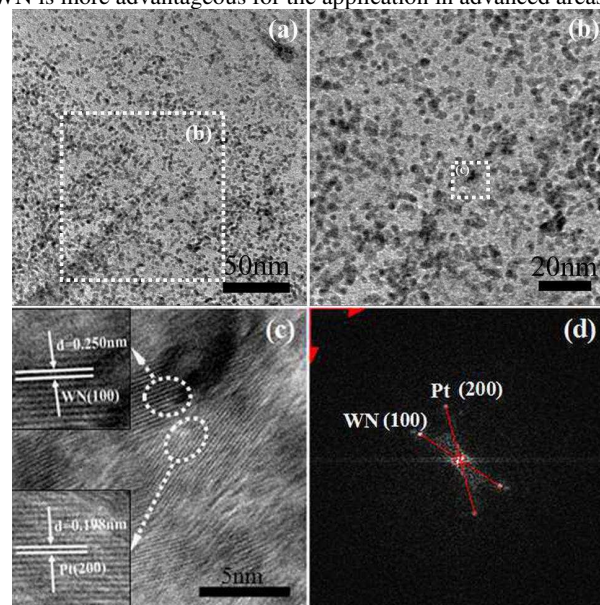


Figure 3. (a, b) low-magnified TEM images, (c) HRTEM and (d) FFT image of Pt-WN/graphene.

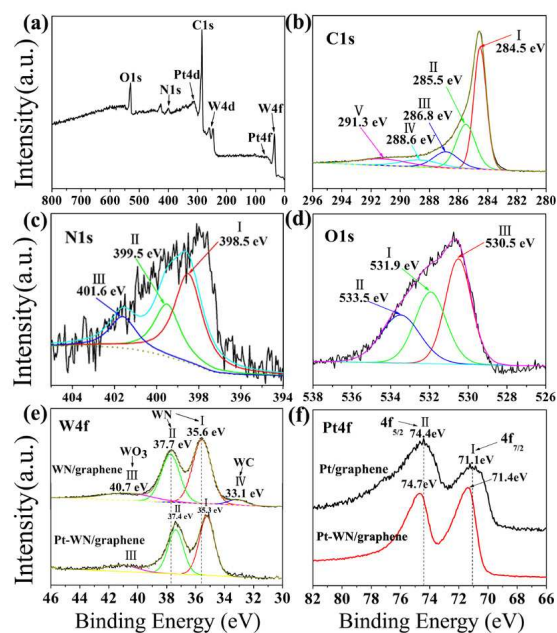


Figure 4. (a-d) XPS spectra of Pt-WN/graphene catalyst: (a) wide scan, (b) C1s, (c) N1s, and (d) O1s; (e) W4f of WN/graphene and Pt-WN/graphene; (f) Pt4f of Pt/graphene and Pt-WN/graphene.

5 The structure of Pt-WN/graphene is analyzed by X-ray photoelectron spectrum (XPS). As shown in Figure 4a, the peaks belonging to C, O, N, W and Pt can be clearly seen in the wide scan spectra. The C1s spectra of the sample can be deconvoluted into five sub-peaks labeled with I, II, III, IV and V as shown in Figure 4b. Peak I represents graphitic carbon with C-C, C=C and C-H bonds at a binding energy (BE) of 284.5 eV.^[38] Other four small peaks at higher binding energy indicate the existence of carbon combined with nitrogen and oxygen groups. Specifically, Peak II (285.5 eV) is ascribed to the carbon in C-N bond.^[42] The formation of C-N bond should be attributed to the reaction of NH₃ with the carbon in graphene. This indicates that during the nitridation process, the NH₃ can react both with tungsten to form the N-W bond and react with C to make N doping. The peak III, IV and V can be indexed to the carbon from C-O bond (286.8 eV), C=O bonds (288.6 eV) and carboxyl group (O=C-O) (291.3 eV), respectively.^[43] As shown, the carbon combined with O in the original GO have much higher peaks than that in Pt-WN/graphene (Figure S10). The result indicates the removal of oxygen-containing groups in GO to form GO-derived graphene in the preparation. The N1s spectrum in Figure 4c can be deconvoluted into three peaks. The Peak I (398.5 eV) is ascribed to the N from WN. The Peak II (399.5 eV) and III (401.6 eV) is derived from the N atoms combining with C atoms in graphene. In detail, the Peak II can be ascribed to the pyrrolic/pyridine N, and Peak III is indexed to the quaternary N.^[44] The results from N spectra are consistent with that from the carbon spectra. It has been reported that nitrogen doping can induce a lot of defects within the graphene structure. After nitridation, the ratio of I_D/I_G ratio in Raman spectra has increased obviously (Figure S1). This implies also nitrogen doping on the graphene,^[45] being consistent with above analyses. In O1s spectra, we can observe the oxygen peak from C=O (531.9 eV, peak I), the hydroxyl O-H (533.5 eV, peak II). Besides, the weak peak at 530.5 eV (Peak III) is

ascribed to oxygen from the W-O.^[46] However, the WO₃ phase can not be reflected in the XRD pattern. This suggests the low amount or amorphous characteristics of WO₃ in the composite. The W4f spectrum shows that W from W-N (35.3 eV) is predominated component in Pt-WN/graphene, but less amount W from W-O also appears at 40.7 eV. The existence of W-O confirms further the result of oxygen spectra. The interaction between different components is a particular focus that directly affects the performance of a composite. Besides the component and valence of elements, the XPS can also give the information about interfacial interaction between the components.^[47] To give the some information about the interaction of Pt and WN in Pt-WN/graphene, XPS spectra of two other samples, Pt/graphene and WN/graphene, are also given. For WN/graphene, the peak of W from W-N locates at 35.6 and 37.7 eV. The W4f BE for ternary Pt-WN/graphene is 35.3 and 37.4 eV, having a negative shift relative to that of WN/graphene. The shift can be explained by the electron transfer^[48] between Pt and WN due to intimately contact and intensive interaction as shown by TEM and XRD test. The interaction is reflected also by comparing the Pt spectrum of Pt-graphene with that of Pt-WN/graphene. As shown, the Pt 4f spectrum of Pt/graphene shows one doublet with Pt 4f_{7/2} binding energy of 71.1 eV and Pt 4f_{5/2} binding energy of 74.4 eV. The Pt 4f spectrum of Pt-WN/graphene shows positive shift of 0.3 eV (71.4 and 74.7 eV) in comparison with that of Pt/graphene. It further indicates the existence of electron interaction between Pt and WN (the transfer of electrons is from Pt to WN). The XAFS measurement is also performed to furtherly confirm the interaction between Pt and WN in Pt-WN/graphene catalyst. The W L3-edge white line mostly derives from electron transitions from the 2p_{3/2} state to a vacant 5d state.^[49] We can see that the peaks center at 10207.5 eV and 10208.1 eV for WN/Graphene and Pt-WN/graphene (Figure S11). A negative shift of 0.6 eV can be observed after Pt growth on WN/graphene. In our previous work, a positive shift of Ti L-edge was observed in TiO₂/graphene in comparison with pure TiO₂, which was contributed into the electron transfer from TiO₂ to graphene.^[50] So, the negative shift indicates the acquisition of the electron of WN after Pt growth, implying the electron transfer from Pt to WN in ternary Pt-WN/graphene. The result of XAFS is consistent with that of XPS. By combination the results of XAFS and XPS, we can confirm the existence of the interaction between Pt and WN in ternary Pt-WN/Graphene catalyst. The strong interaction is significant for improving the performance of catalyst in electrocatalytic application.^[51]

Electrochemical tests

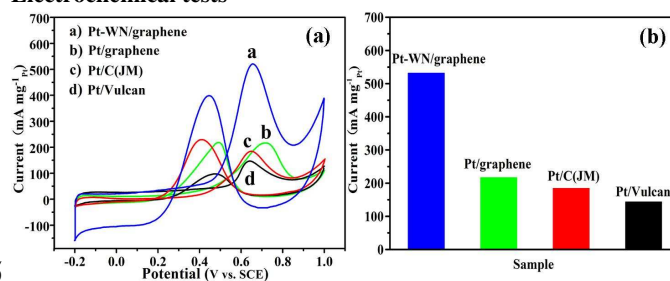


Figure 5. (a) Cyclic voltammograms for methanol electro-oxidation of different catalysts recorded in aqueous 1.0 M H₂SO₄ + 1.0 M CH₃OH solution with a sweep rate of 50 mVs⁻¹ and (b) Mass activity of different catalysts.

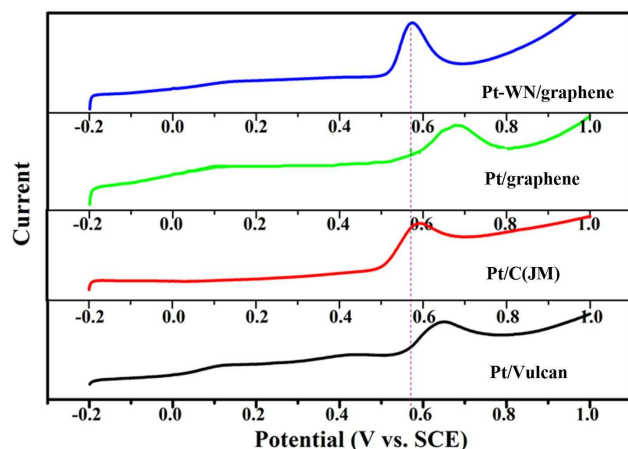


Figure 6. CO-stripping curves of different catalyst in N_2 -protecting 1 M H_2SO_4 solution at a scan rate of 20 mVs^{-1} . The Pt-WN/graphene has the lowest peak potential of 0.57 V that is 20 mV, 100 mV and 80 mV more negative than that for Pt/C(JM), Pt/graphene and Pt/vulcan carbon.

5

The promising characteristics of small size of nitrides, intimate contact and intensive interaction of Pt with WN are largely favorable to enhance the catalytic performance of Pt catalyst. We evaluate the electrocatalytic performance of ternary Pt-WN/graphene toward the methanol electro-oxidation reaction (the heart react of DMFC technology). A suitable catalyst should have a higher induced current density and good stability at a given applied potential. Figure 5a and 5b show the cyclic voltammetry (CV) curves for methanol electro-oxidation and the mass activity of the different catalysts. The performance of Pt/graphene, Pt/C(JM), and Pt/Vulcan are tested as control. The mass activity of Pt-WN/graphene, Pt/graphene, Pt/C(JM), and Pt/Vulcan are $531.5\text{ mA mg}^{-1}_{Pt}$ at 0.65 V, $216.9\text{ mA mg}^{-1}_{Pt}$ at 0.72V, $184.5\text{ mA mg}^{-1}_{Pt}$ at 0.65V, $143.6\text{ mA mg}^{-1}_{Pt}$ at 0.65V. We can see that the ternary Pt-WN/graphene gives highest mass activity, which is 2.45, 2.88 and 3.70 times of Pt/graphene, Pt/C(JM) and Pt/Vulcan, respectively. At the same time, for WN/graphene, no peaks of methanol oxidation are observed, indicating that WN NPs have no catalytic activity and only play the cocatalytic role. The ternary Pt-WN/graphene catalyst prepared by using GO without PEI modification as support have shown poor catalytic activity, further indicating the important role of PEI in the synthesis of WN/graphene with the promoted synergistic effect (Figure S12). Meanwhile, Goodenough et al.^[52] suggested the anodic peak in the reverse scan is relative to the removal of the incomplete oxidized carbonaceous species, such as CO and $HCOO^-$, that accumulated on the catalyst surface during the forward anodic scan. CO, a critical intermediate of methanol oxidation, can poison the Pt catalyst, thus decrease the fuel cell potential and energy conversion efficiency. Consequently, the ratio of the forward anodic peak current density (I_f) to the backward anodic peak current density (I_b), I_f/I_b , can be also used to indicate the CO tolerance of the catalyst. A higher I_f/I_b ratio is indicative to improved CO tolerance.^[53] It can be clearly seen that the Pt-WN/graphene shows a higher ratio of I_f/I_b (1.33) compared to Pt/C (JM) ($I_f/I_b=0.88$) and Pt/graphene ($I_f/I_b=0.99$). The good CO tolerance of Pt-WN/graphene is further demonstrated by CO stripping tests in 1 M H_2SO_4 at room temperature (Figure 6). We can see that the peak potential of Pt-WN/graphene, Pt/graphene, Pt/C(JM) and Pt/vulcan carbon are 0.57 V, 0.67 V, 0.59 V and 0.65 V, respectively. Generally, more lower potential of CO oxidation corresponds to the more better CO tolerance of a catalyst.^[54] Obviously, the Pt-WN/graphene has the lowest peak potential of 0.57 V that is 20 mV, 100 mV and 80 mV more

10

15

20

25

30

35

40

45

50

negative than that for Pt/C(JM), Pt/graphene and Pt/vulcan carbon. The results confirm the excellent electrocatalytic activity of Pt-WN/graphene (high mass activity and good CO tolerance). A smaller amount of Pt is required for Pt-WN/graphene to generate the same current, and a substantial amount of Pt can be saved. The high catalytic activity of Pt-WN/graphene can be attributed to the intimately contact and intensive interaction of the Pt with WN for enhanced synergistic effect. To understand the high activity of Pt-WN/graphene deeply, the BET specific surface area (S_{BET}) of different catalyst are also test as its large effect on the catalytic activity of catalysts. The S_{BET} are $263.2\text{ m}^2\text{ g}^{-1}$, $50.4\text{ m}^2\text{ g}^{-1}$, $170\text{ m}^2\text{ g}^{-1}$, $151\text{ m}^2\text{ g}^{-1}$ for Pt-WN/graphene, Pt/graphene, Pt/C(JM) and Pt/vulcan (Table S1). The Pt-WN/graphene has highest SSA, so it can provide the large accessible interfaces in electrochemical reaction, which is also favorable for enhancing the catalytic activity of ternary catalyst.

65

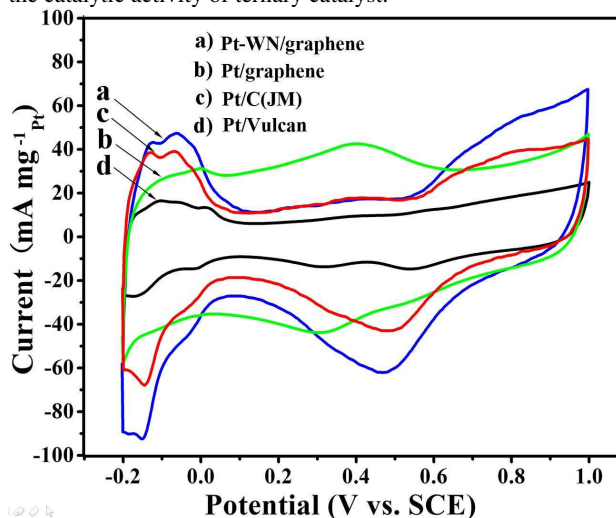


Figure 7. CV curves recorded in N_2 -purged 1.0 M aqueous H_2SO_4 with a sweep rate of 50 mVs^{-1} . The calculated electrochemically active surface area (ECSA) of Pt-WN/graphene, Pt/graphene, Pt/C(JM), and Pt/Vulcan are $88.43\text{ m}^2\text{ g}^{-1}_{Pt}$, $18.08\text{ m}^2\text{ g}^{-1}_{Pt}$, $74.33\text{ m}^2\text{ g}^{-1}_{Pt}$ and $33.99\text{ m}^2\text{ g}^{-1}_{Pt}$.

70

75

80

85

90

Figure 7 shows the CV curves of the four catalysts recorded in N_2 -purged 1.0 M H_2SO_4 . The electrochemically active surface area (ECSA) of Pt-WN/graphene, Pt/graphene, Pt/C(JM), and Pt/Vulcan are $88.43\text{ m}^2\text{ g}^{-1}_{Pt}$, $18.08\text{ m}^2\text{ g}^{-1}_{Pt}$, $74.33\text{ m}^2\text{ g}^{-1}_{Pt}$ and $33.99\text{ m}^2\text{ g}^{-1}_{Pt}$. The Pt-WN/graphene has the optimal ECSA, which is 4.89, 1.19 and 2.60 times those of Pt/graphene, Pt/C(JM) and Pt/Vulcan catalysts, respectively. Therefore, a smaller amount of Pt is required for Pt-WN/graphene to generate the same current. The stability of Pt-WN/graphene catalyst is a key factor determining its practical application. Chronoamperometric (CA) measurement is used to test the durability of catalysts. Figure 8 gives the CA of Pt-WN/graphene, Pt/graphene, Pt/C(JM) and Pt/Vulcan for methanol oxidation measured in 1.0 M H_2SO_4 containing 1.0 M CH_3OH . The Figure with higher resolution at $t=0s$ is given in Figure S13. The residual currents for Pt-WN/graphene, Pt/graphene, Pt/C(JM) and Pt/Vulcan are $76.5\text{ mA mg}^{-1}_{Pt}$, $10.2\text{ mA mg}^{-1}_{Pt}$, $9.9\text{ mA mg}^{-1}_{Pt}$, and $0.5\text{ mA mg}^{-1}_{Pt}$ after 3600s, respectively. The normalized decay corresponding to the current at 3600s and initial ($I_{3600s}/I_{initial}$) are $76.5/550 = 0.14$ for Pt-WN/graphene, $10.2/218 = 0.047$ for Pt/graphene, $9.9/216=0.047$ for Pt/C(JM) and $0.5/143=0.0035$ for Pt/vulcan. The Pt-WN/graphene shows small delay and high residual current.

After longer exposure time of 7200 s, we can still see the high residual current of $26.5 \text{ mA mg}^{-1}_{\text{Pt}}$ for Pt-WN/Graphene catalyst. The $I_{7200\text{s}}/I_{\text{initial}}$ are 0.048, 0.021, 0.022 and 0.0025 for Pt-WN/graphene, Pt/graphene, Pt/C (JM) and Pt/vulcan, respectively, demonstrating furtherly the good stability of Pt-WN/graphene (Figure S14). Our tests also show that the electrocatalytic activity and stability of Pt-WN/graphene is more superior to commercial Pt black (JM) catalyst with SSA of $28 \text{ m}^2 \text{ g}^{-1}$ (Figure S15 and Table S1). Even after longer time of 15000s, the Pt-WN/graphene shows still small delay ($I_{15000\text{s}}/I_{\text{initial}}$ is 0.012) and high residual current of $6.5 \text{ mA mg}^{-1}_{\text{Pt}}$, being superior to other catalysts (Figure S16, S17). Furthermore, the CA of Pt-WN/graphene at other potentials is also tested, including 0.45 V, 0.55 V and 0.75 V to study the stability of Pt-WN/graphene (Figure S18). For comparison, the value tested at 0.65V is also added. The I_{initial} is about 141, 396 and $518 \text{ mA mg}^{-1}_{\text{Pt}}$, and $I_{3600\text{s}}$ is 60, 71 and $64 \text{ mA mg}^{-1}_{\text{Pt}}$ at 0.45 V, 0.55 V and 0.75 V. The $I_{3600\text{s}}/I_{\text{initial}}$ are 0.43, 0.18 and 0.12 at 0.45 V, 0.55 V and 0.75 V, respectively. We can see that the ternary catalyst shows good stability at different potential. It indicates that the more low potential results in more good stability. Nevertheless, the catalyst has highest $I_{3600\text{s}}$ and I_{initial} at 0.65 V. The CA test indicates the good stability and high activity of Pt-WN/graphene catalyst. The good durability of ternary catalyst is also demonstrated by TEM images of Pt-WN/graphene and Pt/C (JM) catalyst before and after the electrochemical test. From Figure S19 we can see that particles in Pt-WN/graphene composites have no obvious change before and after electrochemical test. However, for Pt/C(JM), the Pt NPs show a clear aggregation after test. The results demonstrate also the favorable stability of Pt-WN/graphene. The Pt-WN/graphene after electrochemical test is also analyzed by EELS and Raman, in addition to TEM, to study its stability more deeply. The $\text{Nsp}^2\%$ for Pt-WN/graphene have slight decrease before (83%) and after (79%) electrochemical test (Figure S20 and Table S2). In addition, there is no obvious change about Raman spectra of Pt-WN/graphene before and after test, indicating also the good stability of Pt-WN/graphene (Figure S21).

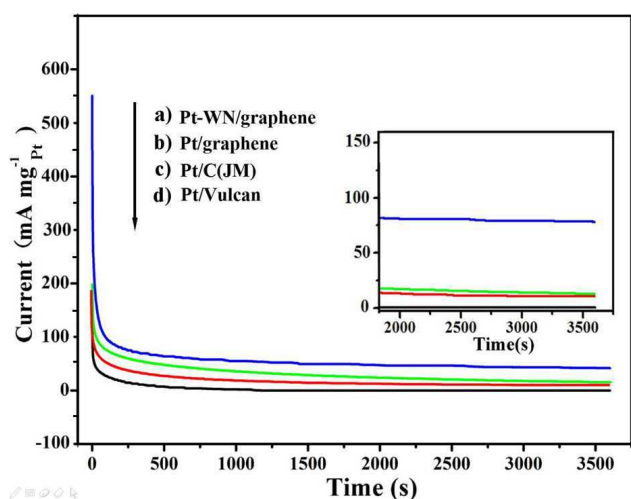


Figure 8. Chronoamperometric curves of different catalysts tested at 0.65V. The inset is the magnified CA curves. The residual currents for the Pt-WN/graphene, Pt/graphene, Pt/C(JM) and Pt/Vulcan are $76.5 \text{ mA mg}^{-1}_{\text{Pt}}$, $10.2 \text{ mA mg}^{-1}_{\text{Pt}}$, $9.9 \text{ mA mg}^{-1}_{\text{Pt}}$, and $0.5 \text{ mA mg}^{-1}_{\text{Pt}}$ after 3600s.

Conclusions

An effective method was developed for loading the small sized WN of 2-3 nm on GO-derived graphene. The use of SiW_{12} clusters as W source and the pre-modification of GO with PEI played the key role in the formation of the small-sized WN on graphene. The WN/graphene could be used as high-effective cocatalyst of Pt NPs for methanol electro-oxidation. The intimate contact (preferentially growth of Pt around WN) and intensive interaction of Pt with WN were observed in the ternary Pt-WN/graphene composites. As the electrocatalyst for oxidation of methanol, the Pt-WN/graphene composite exhibited a remarkably enhanced catalytic performance, such as the higher catalytic activity and stability compared with Pt/graphene, Pt/C (JM) and Pt/Vulcan. The good performance was relative with intimate contact and intensive interaction of Pt with WN in the catalyst. Due to diversity in size, composition and function of POMs, it is believed that the strategy developed here provided an indicative for the synthesis of other metal nitrides (MoN, VN etc.) or mixed nitrides for the application in the advanced areas.

Acknowledgements

We gratefully acknowledge the support of this research by the Key Program Projects of the National Natural Science Foundation of China (No 21031001), the National Natural Science Foundation of China (91122018, 21371053, 21101061), the Cultivation Fund of the Key Scientific and Technical Innovation Project, Ministry of Education of China (No 708029), Program for Innovative Research Team in University (IRT-1237), Special Research Fund for the Doctoral Program of Higher Education of China (20112301110002), Youth Foundation of Heilongjiang Province of China (QC2010021). The authors thank beamline BL14W1 (Shanghai Synchrotron Radiation Facility). The authors thank Prof. Jianqiang Wang for his help on XAFS analysis. The authors appreciate greatly the Prof. Dangsheng Su and Dr. Zhenbao Feng for their useful analysis and help on EELS.

Notes and references

Key Laboratory of Functional Inorganic Material Chemistry, Ministry of Education of the People's Republic of China, Heilongjiang University, Harbin 150080 (P. R. China), Fax: (+ 86) 451-8666-1259
E-mail: fuhg@vip.sina.com; chunguitianhq@163.com

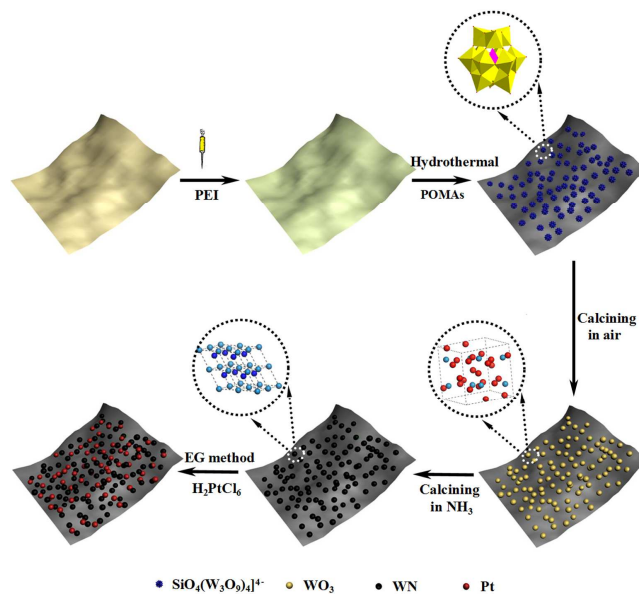
†Electronic Supplementary Information (ESI) available: [details of any supplementary information available should be included here]. See DOI: 10.1039/b000000x/

‡ Footnotes should appear here. These might include comments relevant to but not central to the matter under discussion, limited experimental and spectral data, and crystallographic data.

- [1] a) M. K. Debe, *Nature*, 2012, **486**, 43–51; b) Z. W. Chen, D. Higgins, A. P. Yu, L. Zhang and J. J. Zhang, *Energy Environ. Sci.*, 2011, **4**, 3167–3192; c) C. Hartnig, L. Jorissen, W. Lehnert and J. Scholta, in *Materials for Fuel Cells*, ed. M. Gasik, Woodhead Publishing, Oxford, UK, 2008, ch. 9, pp. 185–208;
- [2] a) A. Rabis, P. Rodriguez and T. J. Schmidt, *ACS Catal.*, 2012, **2**, 864–890; b) Y. H. Bing, H. S. Liu, L. Zhang, D. Ghosha and J. J. Zhang, *Chem. Soc. Rev.*, 2010, **39**, 2184–2202.
- [3] a) K. P. Gong, F. Du, Z. H. Xia, M. Durstock and L. M. Dai, *Science*, 2009, **323**, 760–764; b) P. Chen, T. Y. Xiao, Y. H. Qian, S. S. Li and S. H. Yu, *Adv. Mater.*, 2013, **25**, 3192–3196; c) Y.

- Jiao, M. Jaroniec and S. Z. Qiao, *Angew. Chem. Int. Ed.*, 2012, **51**, 11496–11500; d) H. B. Wang, T. Maiyalagan and X. Wang, *ACS Catal.*, 2012, **2**, 781–794.
- [4] H. J. Tang, H. J. Yin, J. Y. Wang, N. L. Yang, D. Wang and Z. Y. Tang, *Angew. Chem. Int. Ed.*, 2013, **52**, 5585–5589.
- [5] a) C. Koenigsmann, D. B. Semple, E. Sutter, S. E. Tobierre and S. S. Wong, *ACS Appl. Mater. Interfaces*, 2013, **5**, 5518–5530; b) C. Koenigsmann and S. S. Wong, *Energy Environ. Sci.*, 2011, **4**, 1161–1176; c) L. H. Li, Y. Wu, J. Lu, C. Y. Nan and Y. D. Li, *Chem. Commun.*, 2013, **49**, 7486–7488; d) E. Taylor, S. T. Chen, J. Tao, L. J. Wu, Y. M. Zhu and J. Y. Chen, *ChemSusChem*, 2013, **6**, 1863–1867; e) H. J. Qiu and F. X. Zou, *ACS Appl. Mater. Interfaces*, 2012, **4**, 1404–1410.
- [6] a) J. S. J. Hargreaves, *Coord. Chem. Rev.*, 2013, **257**, 2015–2031; b) R. B. Levy and M. Boudart, *Science*, 1973, **181**, 547–549.
- [7] a) Y. Liu, T. G. Kelly, J. G. Chen and W. E. Mustain, *ACS Catal.*, 2013, **3**, 1184–1194; b) J. G. Chen, *Chem. Rev.*, 1996, **96**, 1477–1498.
- [8] a) S. Sharma and B. G. Pollet, *J. Power Sources*, 2012, **208**, 96–119; b) Z. J. Mellinger, T. G. Kelly and J. G. Chen, *ACS Catal.*, 2012, **2**, 751–758.
- [9] G. F. Cui, P. K. Shen, H. Meng, J. Zhao and G. Wu, *J. Power Sources*, 2011, **196**, 6125–6130.
- [10] a) C. H. Liang, L. Ding, C. Li, M. Pang, D. S. Su, W. Z. Li and Y. M. Wang, *Energy Environ. Sci.*, 2010, **3**, 1121–1127; b) C. G. Tian and H. G. Fu, *Rev. Adv. Sci. Eng.*, 2013, **2**, 57–76.
- [11] D. J. Ham and J. S. Lee, *Fuel Cell*, 2009, **2**, 873–899.
- [12] a) L. Wang, J. Yin, L. Zhao, C. G. Tian, P. Yu, J. Q. Wang and H. G. Fu, *Chem. Commun.*, 2013, **49**, 3022–3024; b) J. Yin, L. Wang, C. G. Tian, T. X. Tan, G. Mu, L. Zhao and H. G. Fu, *Chem. Eur. J.*, 2013, **19**, 13979–13986; c) M. J. Liu, Y. Z. Dong, Y. M. Wu, H. B. Feng and J. H. Li, *Chem. Eur. J.*, 2013, **19**, 14781–14786.
- [13] W. Zheng, T. P. Cotter, P. Kaghazchi, T. Jacob, B. Frank, K. Schlichte, *J. Am. Chem. Soc.* 2013, **135**, 3458–3464.
- [14] N. Hugot, A. Desforges, S. Fontana, J. F. Maréché, C. Hérold, A. Albiñak and G. Furdin, *J. Solid State Chem.*, 2012, **194**, 23–31.
- [15] A. Salamat, A. L. Hector, P. Kroll and P. F. McMillan, *Coord. Chem. Rev.*, 2013, **257**, 2063–2072.
- [16] W. M. Liu, M. Q. Shi, X. L. Lang, D. Zhao, Y. Q. Chu and C. A. Ma, *Catal. Today*, 2013, **200**, 87–93.
- [17] H. A. Wriedt, *Bull. Alloy Phase Diagrams*, 1989, **10**, 358–367.
- [18] a) S. M. Wang, X. H. Yu, Z. J. Lin, R. F. Zhang, D. W. He, J. Q. Qin, J. L. Zhu, J. T. Han, L. Wang, H. Mao, J. Z. Zhang and Y. S. Zhao, *Chem. Mater.*, 2012, **24**, 3023–3028; b) Y. Hara, N. Minami, H. Matsumoto and H. Itagaki, *Appl. Catal., A: General*, 2007, **332**, 289–296; c) C. N. Ma, J. F. Sheng, N. Brandon, C. Zhang and G. H. Li, *Int. J. Hydrogen Energy*, 2007, **32**, 2824–2829.
- [19] a) Special volume on "Polyoxometalates", *Chem. Rev.* 1998, **98**, 1–398; b) Y. F. Wang and I. A. Weinstock, *Chem. Soc. Rev.*, 2012, **41**, 7479–7496.
- [20] D. L. Long, R. Tsunashima and L. Cronin, *Angew. Chem. Int. Ed.*, 2010, **49**, 1736–1758.
- [21] a) D. Chen, L. H. Tang and J. H. Li, *Chem. Soc. Rev.*, 2010, **39**, 3157–3180; b) X. M. Feng, R. M. Li, Y. W. Ma, R. F. Chen, N. E. Shi, Q. L. Fan and W. Huang, *Adv. Funct. Mater.*, 2011, **21**, 2989–2996; c) C. C. Huang, C. Li and G. Q. Shi, *Energy Environ. Sci.*, 2012, **5**, 8848–8868.
- [22] a) Y. M. Tan, C. F. Xu, G. X. Chen, N. F. Zheng and Q. J. Xie, *Energy Environ. Sci.* 2012, **5**, 6923–6927; b) J. Yang, C. G. Tian, L. Wang and H. G. Fu, *J. Mater. Chem.*, 2011, **21**, 3384–3390; c) H. Zhao, J. Yang, L. Wang, C. G. Tian, B. J. Jiang and H. G. Fu, *Chem. Commun.*, 2011, **47**, 2014–2016; d) H. J. Yin, H. J. Tang, D. Wang, Y. Gao and Z. Y. Tang, *ACS Nano*, 2012, **6**, 8288–8297.
- [23] W. S. Hummers and R. E. Offeman, *J. Am. Chem. Soc.*, 1958, **80**, 1339–1339.
- [24] J. Wu, F. Hu, P. K. Shen, C. M. Li and Z. Wei, *Fuel Cell*, 2010, **10**, 106–110.
- [25] E. Karabulut, T. Pettersson, M. Ankerfors and L. Wågberg, *ACS Nano*, 2012, **6**, 4731–4739.
- [26] A. M. Douvas, E. Makarona, N. Glezos, P. Argitis, J. A. Mielczarski and E. Mielczarski, *ACS Nano*, 2008, **2**, 733–742.
- [27] R. H. Wang, Y. Xie, K. Y. Shi, J. Q. Wang, C. G. Tian, P. K. Shen and H. G. Fu, *Chem. Eur. J.*, 2012, **18**, 7443–7451.
- [28] a) R. F. Nie, J. J. Shi, W. C. Du, W. S. Ning, Z. Y. Hou and F. S. Xiao, *J. Mater. Chem. A*, 2013, **1**, 9037–9045; b) A. C. Ferrari, J. C. Meyer, V. Scardaci, C. Casiraghi, M. Lazzeri, F. Mauri, S. Piscanec, D. Jiang, K. S. Novoselov, S. Roth and A. K. Geim, *Phys. Rev. Lett.*, 2006, **97**, 187401.
- [29] Y. Baek and K. J. Yong, *J. Phys. Chem. C*, 2007, **111**, 1213–1218.
- [30] F. Xu, A. Fahmi, Y. Zhao, Y. D. Xia and Y. Q. Zhu, *Nanoscale*, 2012, **4**, 7031–7037.
- [31] S. Bali, T. T. Chen, W. Chaikittisilp and C. W. Jones, *Energy Fuels*, 2013, **27**, 1547–1554.
- [32] H. Y. Ma, Y. Q. Luo, S. X. Yang, Y. W. Li, F. Cao and J. Gong, *J. Phys. Chem. C*, 2011, **115**, 12048–12053.
- [33] J.-O. Müller, D. S. Su, U. Wild and R. Schlögl, *Phys. Chem. Chem. Phys.*, 2007, **9**, 4018–4025.
- [34] A. Kafizas, C. J. Carmalt and I. P. Parkin, *Coord. Chem. Rev.*, 2013, **257**, 2073–2119.
- [35] Z. W. Yao, X. H. Zhang, F. Peng, H. Yu, H. J. Wang and J. Yang, *J. Mater. Chem.*, 2011, **21**, 6898–6902.
- [36] R. H. Wang, C. G. Tian, L. Wang, B. L. Wang, H. B. Zhang and H. G. Fu, *Chem. Commun.*, 2009, **45**, 3104–3106.
- [37] J. Yang, Y. Xie, R. H. Wang, B. J. Jiang, C. G. Tian, G. Mu, J. Yin, B. Wang and H. G. Fu, *ACS Appl. Mater. Interface*, 2013, **5**, 6571–6579.
- [38] D. M. Fernandes, C. M. A. Brett and A. M. V. Cavaleiro, *J. Solid State Electrochem.*, 2011, **15**, 811–819.
- [39] J. F. Wang, J. X. Gong, Y. S. Xiong, J. D. Yang, Y. Gao, Y. L. Liu, X. Q. Lu and Z. Y. Tang, *Chem. Commun.*, 2011, **47**, 6894–6896.
- [40] a) C. Y. He, H. Meng, X. Y. Yao and P. K. Shen, *Int. J. Hydrogen Energy*, 2012, **37**, 8154–8166; b) Z. X. Yan, M. Cai and P. K. Shen, *Sci. Rep.*, 2013, **3**, 1646–1652.
- [41] a) Z. X. Yan, H. G. Wang, M. P. Zhang, Z. F. Jiang, T. S. Jiang and J. M. Xie, *Electrochimica Acta.*, 2013, **95**, 218–224; b) R. H. Wang, J. Yang, K. Y. Shi, B. Wang, L. Wang, G. H. Tian,

- B. Bateer, C. G. Tian, P. K. Shen and H. G. Fu, *RSC Adv.*, 2013, **3**, 4771–4777.
- [42] A. J. Patil, J. L. Vickery, T. B. Scott and S. Mann, *Adv. Mater.*, 2009, **21**, 3159–3164.
- 5 [43] S. Ababou-Girard, H. Sabbah, B. Fabre, K. Zellama, F. Sola and C. Godet, *J. Phys. Chem. C*, 2007, **111**, 3099–3108.
- [44] a) K. Artyushkova, B. Kiefer, B. Halevi, A. Knop-Gericke, R. Schlogl and P. Atanassov, *Chem. Commun.*, 2013, **49**, 2539–2541; b) L. Sun, C. G. Tian, Y. Fu, Y. Yang, J. Yin, L. Wang and
- 10 H. G. Fu, *Chem. Eur. J.*, 2014, **20**, 564–574.
- [45] C. H. Zhang, L. Fu, N. Liu, M. H. Liu, Y. Y. Wang and Z. F. Liu, *Adv. Mater.*, 2011, **23**, 1020–1024.
- [46] Y. D. Zhang, W. W. He, H. X. Zhao and P. J. Li, *Vacuum*, 2013, **95**, 30–34.
- 15 [47] P. S. Bagus, E. S. Ilton and C. J. Nelin, *Surf. Sci. Rep.*, 2013, **68**, 273–304.
- [48] A. L. Wang, H. Xu, J. X. Feng, L. X. Ding, Y. X. Tong and G. R. Li, *J. Am. Chem. Soc.*, 2013, **135**, 10703–10709.
- [49] S. Yamazoe, Y. Hitomi, T. Shishido and T. Tanaka, *J. Phys. Chem. C*, 2008, **112**, 6869–6879.
- 20 [50] B. J. Jiang, C. G. Tian, Q. J. Pan, Z. Jiang, J. Q. Wang, W. S. Yan and H. G. Fu, *J. Phys. Chem. C*, 2011, **115**, 23718–23725.
- [51] Z. X. Yan, G. Q. He, M. Cai, H. Meng and P. K. Shen, *J. Power Sources*, 2013, **242**, 817–823.
- 25 [52] R. Manohara and J. B. Goodenough, *J. Mater. Chem.*, 1992, **2**, 875–887.
- [53] S. H. Sun, G. X. Zhang, N. Gauquelin, N. Chen, J. G. Zhou, S. L. Yang, W. F. Chen, X. B. Meng, D. S. Geng, M. N. Banis, R. Y. Li, S. Y. Ye, S. Knights, G. A. Botton, T.K. Sham and X. L.
- 30 Sun, *Sci. Rep.*, 2013, **3**, 1775–1793.
- [54] a) H. Yuan, D. Guo, X. Li, L. Yuan, W. Zhu, L. Chen and X. Qiu, *Fuel Cell*, 2009, **9**, 121–127; b) F. Maillard, F. Gloaguen and J. M. Leger, *J. Appl. Electrochem.*, 2003, **33**, 1–8.



The WN of 2-3 nm is grown on the graphene, which can be used as promising carriers for methanol electro-oxidation.

Broader context:

Transition metal nitrides are attracting much more attention in material science because of their unique properties for technological applications. In the field of direct methanol fuel cells (DMFC), the nitrides are promising co-catalyst of Pt metal. The co-catalytic role is severely affected by their size and dispersion on supports. The small size and uniform distribution can increase largely the chance of nitrides to contact with Pt, thus promote the development of the synergistic catalytic action. However, the preparation of the nitrides with these characteristics remains a large challenge to date. Polyoxometalates (POMs) are a famous class of molecular clusters with much diversity in size, composition and function. The small size close to the nanometer, stable structure of POMs clusters make them suitable precursor for preparing the WN with small size. In this paper, we report the synthesis of the small-sized WN nanoparticles (NPs) loading on GO-derived graphene by using heteropoly acid $H_4[SiO_4(W_3O_9)_4]$ (SiW_{12}) clusters as W source. The WN/graphene can be used as promising carriers of Pt for methanol electro-oxidation, with enhanced activity, excellent resistance to CO poisoning and durability.